Bull. Mater. Sci. (2019) 42:77
https://doi.org/10.1007/s12034-019-1743-2

Comparative studies on spinal ferrite MFe_2O_4 (M = Mg/Co) nanoparticles as potential adsorbents for Pb(II) ions

PALAK JAIN, MANPREET KAUR, MANMEET KAUR* and JASPREET KAUR GREWAL
Department of Chemistry, Punjab Agricultural University, Ludhiana 141 004, India
*Author for correspondence (manmeetgill885@gmail.com)

MS received 9 May 2018; accepted 14 August 2018; published online 7 March 2019

Abstract. Ferrite nanoparticles (NPs) with composition MFe_2O_4 (M = Mg/Co) were synthesized by a facile combustion method. NPs were characterized employing various physico-chemical techniques. X-ray diffraction patterns confirmed the phase purity, transmission electron micrographs indicated that NPs are spherical and average diameter of maximum fraction of NPs was in the range of 20–30 nm. Magnetic studies revealed that the saturation magnetization values for $MgFe_2O_4$ and $CoFe_2O_4$ NPs were 13.17 and 41.12 emu g^{-1}, respectively. The Brunauer–Emmett–Teller surface area of $CoFe_2O_4$ and $MgFe_2O_4$ NPs was 22.98 and 34.39 m^2 g^{-1}, respectively. Synthesized ferrite NPs and activated charcoal were comparatively analysed as adsorbents for removal of Pb(II) ions. The factors influencing uptake behaviour of Pb(II) ions *viz*. adsorbent dose, pH, concentration, temperature and contact time were quantified. The adsorption data showed good correlation with Langmuir and Freundlich models as compared to Dubinin–Radushkevich model. The maximum adsorption capacity displayed a two-fold increase for NPs as compared to activated charcoal. The easy magnetic separation of ferrite NPs from the solution and their regeneration with 0.1 N NaOH for reuse without any loss make them potential adsorbents. The trend in ascending order for the elimination of Pb(II) ions from the solution was activated charcoal < $CoFe_2O_4$ NPs < $MgFe_2O_4$ NPs. The observed differences in the adsorption potential of NPs are explained on the basis of structural and magnetic properties and the surface area of NPs.

Keywords. Adsorption; Pb(II) ions; ferrite nanoparticles; TEM; X-ray diffraction.

1. Introduction

The excessive use of heavy metals has substantially increased their concentration in the aquatic environment. It is a problem of global environmental concern. The term heavy metal includes toxic elements having density greater than 3.5–6.0 g cm^{-3} and some metalloids such as arsenic and selenium [1,2]. Heavy metals are non-biodegradable and should be removed from the wastewater to prevent their entry into the food chain. Pb(II) is an accumulative poison added to the aquatic system from anthropogenic and industrial activities e.g., metal plating, tanneries, oil refining and mining [3]. Its bioaccumulation poses elevated risk to human health and causes sterility, abortion, still births and neonatal deaths.

The traditional methods such as reverse osmosis, ion exchange, adsorption, electrolytic recovery, chemical precipitation, ultra-filtration, electro-dialysis and foam floatation and solvent extraction are used for the removal of heavy metals from aqueous solution [4–9]. Among these methods, adsorption is a promising approach as it serves a highly efficient, cost effective and eco-friendly technique along with ease of operation. Activated carbon is a commonly used adsorbent and there is a need for alternative low cost material as potential sorbent for the removal of heavy metals.

Role of nanotechnology for water purification is a thrust area of research. Nanoparticles (NPs) have a greater number of active sites for the interaction with different chemical species. Owing to their small size and large surface area NPs of metal oxides such as Al_2O_3, TiO_2 and Fe_2O_3 have been used as adsorbents [10]. However, separation of nano-metal oxides from wastewater is a challenging area of research. Among the new generation adsorbent materials developed so far, spinel ferrite NPs have shown tunable morphology, high efficiency, high surface to volume ratio and promising magnetic properties. They have a clear edge over other NPs as adsorbents owing to their magnetic behaviour. Spinel ferrite NPs are mixed metal oxides with iron oxide as their main component. They are even better than Fe_2O_3/Fe_3O_4 NPs due to stronger magnetic properties, higher chemical resistance and larger surface area. Transforming the ferric oxide NPs to ferrites, substantially increases the saturation magnetization and facilitates easier magnetic removal, which is more efficient and selective method for the separation of magnetic nanomaterials from aqueous environment after sorption than conventional approach of filtration or centrifugation. Chemically stable nature of spinel ferrites along with their insolubility in water, high surface area and magnetic separation makes them a potential adsorbent for removing contaminants from

water [11–13]. The lower cost of spinel ferrites is another advantage for their commercial application.

Co-precipitation, sol–gel, precursor and combustion approach are the commonly employed chemical methods for the synthesis of ferrite NPs. Combustion approach is a facile route for synthesis of NPs and involves self-propagating exothermic redox reactions between an oxidizer and a fuel. It is an effective approach for bulk synthesis due to high yield of NPs and ease of synthesis [11] as compared to other methods.

Hou *et al* [13] have studied the adsorptive nature of 3D porous $NiFe_2O_4$ synthesized by sol–gel method for methylene blue dye and heavy metals *viz*. Cu(II), Cr(VI) and Ni(II) and it was observed to be an efficient and reusable adsorbent. Ce(III)-doped $ZnFe_2O_4$ NPs are reported for the removal of Cr(VI) by Kuai *et al* [14]. The uptake of Cr(VI) ions by different transition metal spinel ferrites was studied by Hu *et al* [15]. The adsorption of Pb(II) by γ-Fe_2O_3 was explored by Lagashetty *et al* [16]. Ren *et al* [17] studied the adsorption of Pb(II) and Cu(II) from aqueous solution on magnetic porous ferrospinel $MnFe_2O_4$ prepared by a sol–gel process. Nano-sized $NiFe_2O_4$ and $CoFe_2O_4$ synthesized by hydrothermal method are reported as good adsorbents for removing Pb(II) ions [18]. Reddy and Lee [19] have synthesized 3D porous spinel $NiFe_2O_4$ NPs and used them for remediation of Pb(II) from aqueous solutions. Cutila *et al* [20,21] studied Pb(II) adsorption behaviour of mesoporous $CoFe_2O_4$ NPs synthesized through a precipitation method and mesoporous silica-coated magnetite NPs with *o*-vanillin functionalization. Fang *et al* [22] studied Pb adsorption by ferrite synthesized from steel picking sludge. Kang *et al* [23] used $MgFe_2O_4$ microspheres synthesized by a solvothermal method for Pb(II) adsorptive removal with maximum adsorption capacity of 113 mg g^{-1}. Kaur *et al* [24,25] synthesized the nanocomposites of $MgFe_2O_4$ NPs with bentonite and activated carbon for the adsorptive removal of Cr(VI). The nanocomposites display an increase in adsorption potential as compared to pristine NPs. The effect of divalent cation in the spinel ferrites on their adsorption potential has not been explored yet. In the present study, MFe_2O_4 (M = Mg/Co) NPs were synthesized by a facile combustion process. The adsorption capacity of NPs and activated charcoal for the removal of Pb(II) ions from water was comparatively analysed. Influence of factors on the uptake behaviour such as adsorbent dose, pH, concentration, temperature and contact time was ascertained. Adsorption isotherms, thermodynamics and kinetics were used to describe the phenomenon of adsorption. The observed differences are explained on the basis of magnetic properties and formula units of spinel ferrite NPs.

2. Experimental

All chemicals were of analytical reagent grade and were used without further purification. Deionized water was used to prepare solutions.

$$M(NO_3)_2 + 2Fe(NO_3)_3 + 4C_2H_6N_4O_2 \rightarrow MFe_2O_4 + 8CO_2 + 12N_2 + 12H_2O$$
(M = Mg, Co)

Scheme 1. Synthesis of ferrites by combustion method.

2.1 *Synthesis of ferrite NPs*

Oxalyldihydrazide (ODH) was synthesized by dropwise addition of one mole of diethyl oxalate in two moles of hydrazine hydrate at 273 K with continuous stirring. The white precipitates of ODH were washed with cold water and recrystallized using dimethyl sulphoxide and stored in a vacuum desiccator. Elemental analysis and Fourier transform infrared (FT-IR) spectroscopy was used to establish the identity of ODH. The redox reaction representing the synthesis of ferrite NPs from ODH metal nitrate is given in scheme 1.

Metal nitrates and ODH were mixed in a silica crucible in a stoichiometric ratio keeping Φ (oxidizer/fuel ratio) at unity. The mixture was combusted in a muffle furnace in static air atmosphere at 500°C for three hours to obtain ferrite NPs as the final combustion product.

2.2 *Characterization techniques*

Techniques *viz*. X-ray diffraction (XRD), transmission electron microscopy (TEM), Brunauer–Emmett–Teller (BET) surface area study, scanning electron microscopy with energy dispersive X-ray spectroscopy (SEM-EDS) and vibrating sample magnetometer (VSM) were employed according to standard procedures described by Kaur *et al*. The Pb(II) content was estimated using spectrophotometer and atomic adsorption spectroscopy (AAS) techniques. For spectrophotometric analysis, absorbance measurements were carried out by the dithizone method [26] at 535 nm with UV-1800 Shimadzu UV–Visible spectrophotometer equipped with 1 cm quartz cell. For AAS studies, the method was also standardized using an Avanta 5 Atomic Absorption Spectrometer. The results of AAS were corroborated with the results of spectrophotometric analysis.

2.3 *Density measurements*

Experimental density (d_{exp}) was determined using a pycnometer using xylene as a medium for the synthesized NPs [27]. The formula used for the calculation of XRD density is [28]:

$$d_{exp} = \frac{8M}{Na^3}$$

where N is the Avogadro's number and M is the molecular weight of the sample.

The determination of lattice constant (a) was calculated using the following equation:

$$a = d(h^2 + k^2 + l^2)^{1/2}.$$

The percentage porosity was calculated as follows:

$$\text{Percentage porosity} = \left[1 - d_{\text{exp}}/d_{\text{XRD}}\right] \times 100.$$

Scherrer formula was employed to calculate average particle size (D) [29]:

$$D = \frac{\lambda}{d \cos\theta}$$

where d represents full width at half maximum.

2.4 *Adsorption studies*

A stock solution of 1000 mg l^{-1} concentration of Pb(II) ions was prepared by dissolving 1.6 g of $Pb(NO_3)_2 \cdot 4H_2O$ in 1000 ml deionized water. Working solutions were prepared by dilution of stock solution. The influence of pH (2–10) was evaluated by varying the pH of solution with 0.1 M NaOH and 0.1 M HCl to ascertain the optimum pH. The study of factors such as contact time (5–360 min) and adsorbent dose (0.01–1.00 g) was also carried out. The batch method was used to determine the adsorption of Pb(II) from aqueous solution and 0.1 g adsorbent was added to 100 ml solution concentration ranging from 10 to 500 mg l^{-1} taken in 250 ml glass Erlenmeyer flasks. The solutions were equilibrated at room temperature (25°C) using an orbital shaker which was operated at 100 rpm. To ensure the reproducibility of data, the experiments were done twice. The determination of removal efficiency (E) of adsorbent is as follows:

$$E \text{ (percent removal)} = [(C_0 - C_e)/C_0] \times 100$$

where C_0 is the initial concentration and C_e is the equilibrium concentration of solution in mg l^{-1}. Adsorption data were analysed using Langmuir, Freundlich and Dubinin–Radushkevich (D–R) adsorption isotherms.

2.5 *Thermodynamic parameters*

The solutions of 100 mg l^{-1} (Pb(II)) concentration from the stock solution were prepared and then the pH was adjusted to optimum adsorption pH. Subsequently 100 mg $CoFe_2O_4/MgFe_2O_4$ NPs and activated charcoal were added to each flask. The samples were subjected to shaking at a speed of 100 rpm for 2 h at different temperatures i.e., 15, 25, 35 and 45°C. The mixture was centrifuged and the concentration of Pb(II) was determined.

The changes in free energy ΔG°, enthalpy ΔH° and entropy ΔS° associated with the adsorption process were determined by employing the following equations:

$$\Delta G^\circ = -RT \ln K$$

$$\ln K = -\frac{\Delta H^\circ}{RT} + \frac{\Delta S^\circ}{R}$$

where T is the absolute temperature (K), R is the gas constant (8.314 J mol^{-1} K^{-1}) and K represents equilibrium constant at various temperatures. ΔH° and ΔS° were determined from the intercept and slope of the plot of ln K *vs.* $1/T$.

3. Results and discussion

3.1 *Characterization of magnetic NPs*

FT-IR spectrum of $MgFe_2O_4$ NPs (figure 1a) exhibited mainly two bands in the range 400–700 cm^{-1}. A higher frequency

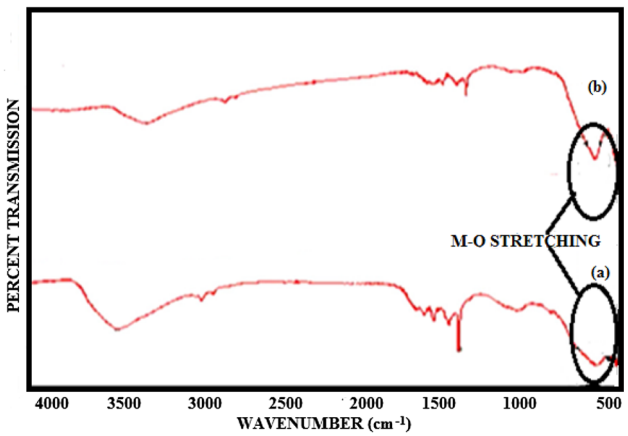

Figure 1. FT-IR spectra of (**a**) $MgFe_2O_4$ and (**b**) $CoFe_2O_4$ NPs.

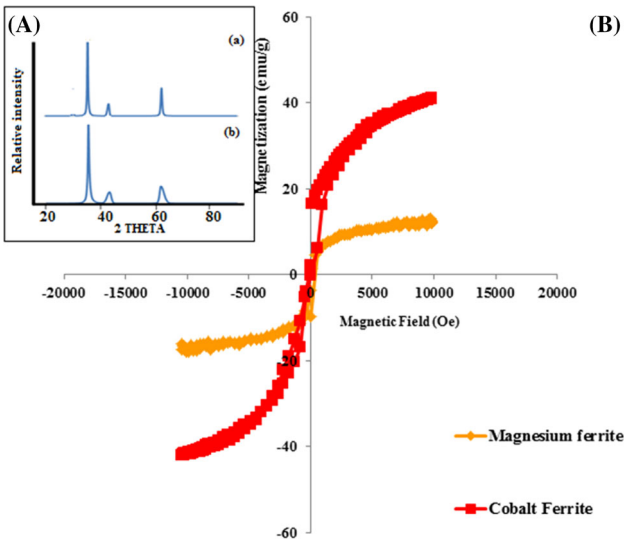

Figure 2. (**A**) XRD patterns of (**a**) $CoFe_2O_4$ and (**b**) $MgFe_2O_4$ NPs and (**B**) hysteresis curves for $MgFe_2O_4$ and $CoFe_2O_4$ NPs.

Table 1. XRD parameters of $MgFe_2O_4$ and $CoFe_2O_4$ NPs.

Composition	Lattice constant (Å)	X-ray density (g cm^{-3})	Physical density (g cm^{-3})	Percentage porosity	Average particle diameter (nm)
$MgFe_2O_4$	8.308 ± 1.21	4.632 ± 0.52	1.508 ± 0.08	10.96 ± 1.90	25.65 ± 2.50
$CoFe_2O_4$	8.297 ± 2.71	5.401 ± 0.83	2.478 ± 0.06	27.36 ± 1.25	31.48 ± 1.65

Table 2. Magnetic parameters of $MgFe_2O_4$ and $CoFe_2O_4$ NPs.

Composition	Saturation magnetization (emu g^{-1})	$4\pi M_s$ (gauss)	Coercivity (Oe)	Remnant magnetization (emu g^{-1})
$MgFe_2O_4$	13.17 ± 0.03	165.49	70 ± 0.37	0.98 ± 0.04
$CoFe_2O_4$	41.12 ± 0.02	516.73	330 ± 0.26	16.22 ± 0.01

band located at 570 cm^{-1} corresponded to the metal ions' stretching vibrations at the tetrahedral site while the lower frequency band observed at 404 cm^{-1} was because of the stretching vibrations in the octahedral site [33]. $CoFe_2O_4$ NPs displayed a similar IR spectrum (figure 1b). The patterns of XRD of the synthesized MFe_2O_4 NPs (M = Mg, Co) clearly showed the formation of fine crystalline single phase ferrite NPs (figure 2A). The phase purity was confirmed by the absence of additional peaks in the XRD pattern. The diffraction patterns displayed peaks for crystallographic planes for $MgFe_2O_4$ and $CoFe_2O_4$ which were also confirmed by matching with the ASTM data cards [30]. Density of the synthesized ferrite NPs was determined from X-ray data and physical method. Porosity values and average particle diameter of NPs are given in table 1. Experimental density was lower as compared to X-ray density. The lower value of density is due to higher porosity in the powdered state. $CoFe_2O_4$ NPs displayed higher values of density as compared to $MgFe_2O_4$ NPs which is corroborated to greater mass of Co^{2+} ions as compared to Mg^{2+} ions. Hysteresis plots represented the magnetization variation (M_s, emu g^{-1}) with magnetic field (H, Oe) (figure 2B). Magnetic parameters *viz.* remnant magnetization (M_r), saturation magnetization (M_s) and coercivity (H_c) (table 2) were in accordance with the reported values in the literature [31,32]. $CoFe_2O_4$ NPs displayed higher M_s values as compared to $MgFe_2O_4$ NPs which resulted in greater agglomeration of $CoFe_2O_4$ NPs in the aqueous solution.

The nitrogen adsorption–desorption isotherms of $MgFe_2O_4$ and $CoFe_2O_4$ NPs were studied using BET analysis which are given in figure 3 along with pore size distribution. The BET surface area for $MgFe_2O_4$ and $CoFe_2O_4$ NPs was found to be 34.39 and 22.98 $m^2\ g^{-1}$, respectively. The higher surface area of $MgFe_2O_4$ NPs can be attributed to the decrease in grain size. Figure 3 also shows the pore size distribution of the synthesized NPs. The average pore diameters of $MgFe_2O_4$ and $CoFe_2O_4$ were 3.00 and 3.15 nm, respectively. These average pore diameters obtained from ferrite NPs are due to the intra-granular pore formed within the metal oxides.

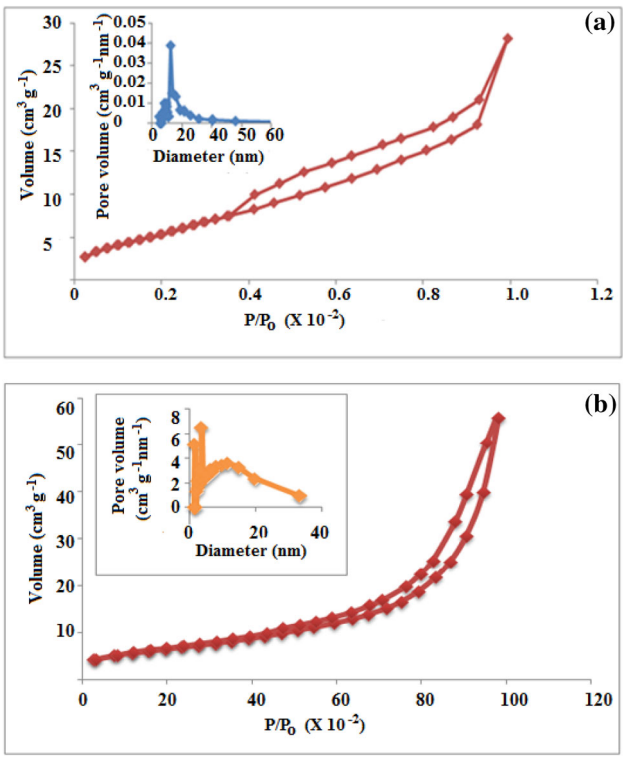

Figure 3. BET of (**a**) $MgFe_2O_4$ and (**b**) $CoFe_2O_4$.

SEM micrograph (figure 4) of $MgFe_2O_4$ NPs confirmed the presence of agglomerates of the NPs in the powdered form which is a distinct feature of magnetic nanomaterials. $CoFe_2O_4$ NPs displayed similar SEM micrographs. TEM images of $MgFe_2O_4$ NPs (figure 5A(a)) clearly displayed the ultrafine spherical NPs forming chains due to magnetic properties. The maximum fraction of particles having size in the range between 20 and 30 nm was observed from the particle size distribution histogram (figure 5A(b)). $CoFe_2O_4$ NPs

displayed similar TEM micrographs (figure 5B(a) and (b)) confirming that both $MgFe_2O_4$ and $CoFe_2O_4$ NPs have similar morphology.

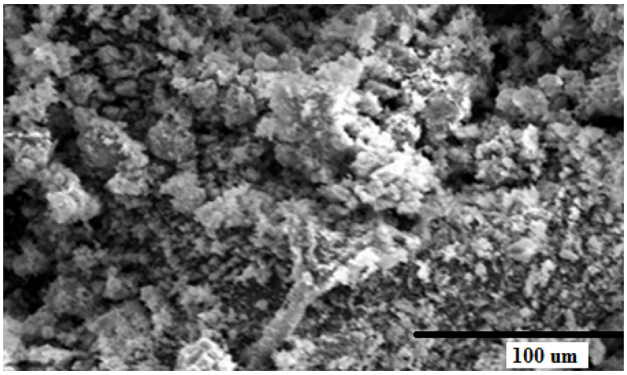

Figure 4. SEM micrograph of $MgFe_2O_4$ NPs.

3.2 *Adsorption studies*

3.2a *Effect of pH*: Solubility of metal ions plays an important role in adsorption as the distribution of species is a function of pH. At low pH, adsorption of Pb(II) on ferrite NPs was low which can be attributed to the competition between H^+ ions and Pb(II) ions for the available sites. At higher pH, the positive surface charge on adsorbent decreased which favoured adsorption. At pH 8, maximum metal uptake was observed (figure 6b). But at pH >8, Pb(II) forms hydro complexes i.e., polymeric hydro complexes predominantly $Pb_4(OH)_4^{4+}$, $Pb_6(OH)_8^{4+}$ and $Pb(OH)_4^{2+}$ decreased the adsorption [34].

3.2b *Effect of contact time*: The effect of contact time on the percent removal of Pb(II) ion is depicted in figure 7. Solutions with a Pb(II) concentration of 10 mg l^{-1} and 0.1 g of

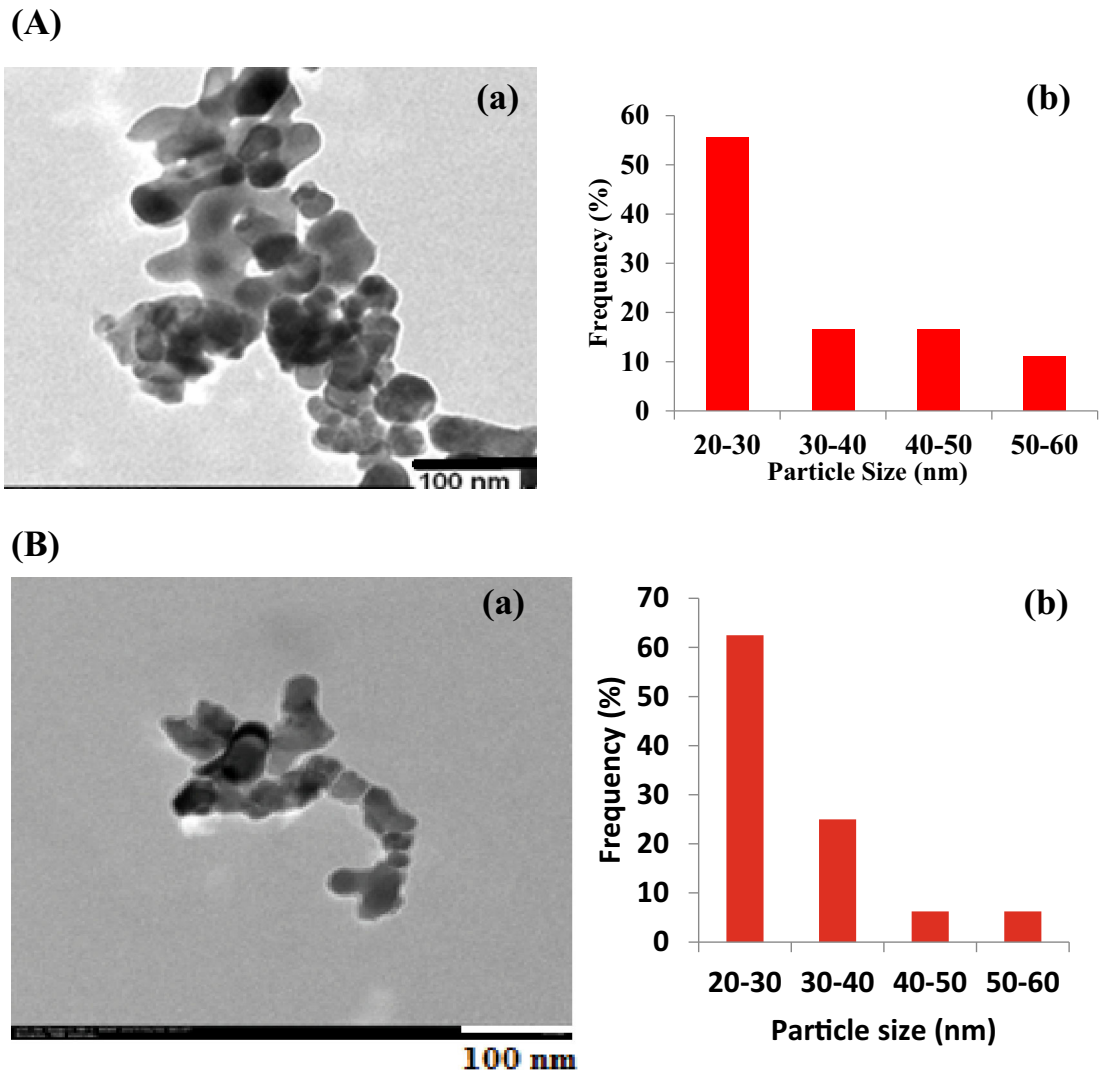

Figure 5. (**A**) (**a**) TEM micrograph of $MgFe_2O_4$ NPs. (**b**) Histogram showing particle size distribution. (**B**) (**a**) TEM micrograph of $CoFe_2O_4$ NPs. (**b**) Histogram showing particle size distribution.

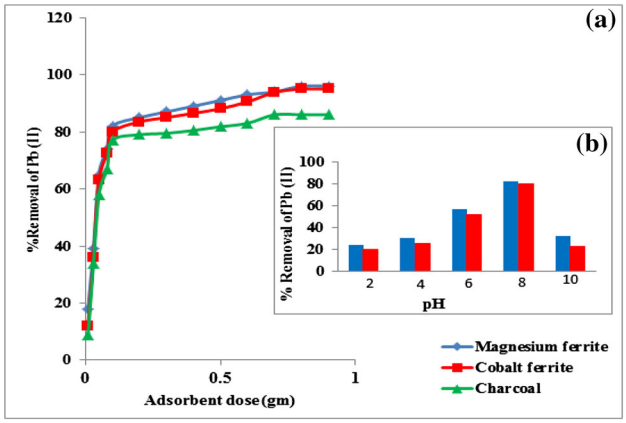

Figure 6. (**a**) Effect of adsorbent dose and (**b**) effect of pH on Pb(II) adsorption by $MgFe_2O_4$ and $CoFe_2O_4$ NPs.

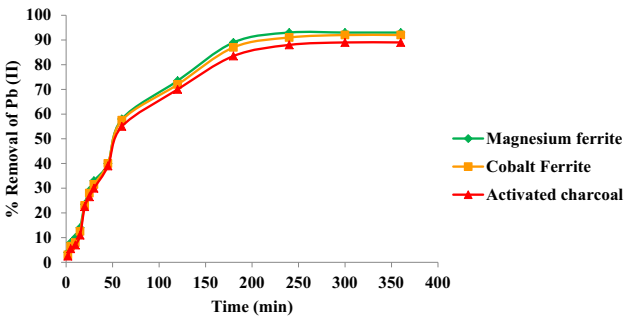

Figure 7. Effect of contact time on Pb(II) adsorption by $MgFe_2O_4$, $CoFe_2O_4$ and activated charcoal.

adsorbent were used for this experiment. For all the three adsorbents adsorption was rapid in the first 60 min as clearly indicated from the slope of the curve and slowed down thereafter as indicated by the flattened curve. In the case of $MgFe_2O_4$ NPs, maximum removal was 93 percent after 4 h. While in the case of $CoFe_2O_4$ NPs and activated charcoal, maximum removal was 92 and 88 percent after 5 h. Pb(II) removal was rapid initially due to availability of vacant sites and the available sites decreased for binding as the contact time was increased. The results are corroborated to magnetic behaviour of the NPs.

3.2c *Effect of adsorbent dose*: The effect of adsorbent dose on the percent removal of Pb(II) ions for 100 mg l^{-1} solution is shown in figure 6a. Percent removal of Pb(II) ions increased at a faster rate initially with an increase in the adsorbent dose up to 0.8 g. A further increase in adsorbent dose did not enhance the removal process and optimum dose for both ferrite NPs was observed as 0.8 g. However, for activated charcoal, optimum dose was 0.9 g. These results confirmed the superiority of ferrite NPs over activated charcoal.

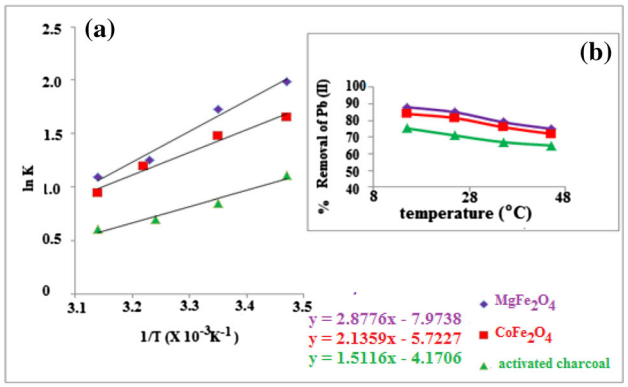

Figure 8. (**a**) Plots of ln K *vs.* $1/T$ for (i) $MgFe_2O_4$, (ii) $CoFe_2O_4$ and (iii) activated charcoal and (**b**) effect of temperature on Pb(II) adsorption.

3.2d *Thermodynamic studies*: Adsorption decreased on increasing the temperature from 15 to 45°C at the interval of 10°C which indicated that the adsorption was accompanied by the evolution of heat (figure 8b). The values of $\Delta H°$ and $\Delta S°$ were evaluated from the intercept and the slope of the plot of ln K *vs.* $1/T$ plots (figure 8a) and are displayed in table 3. The negative $\Delta G°$ values confirmed the favourable and the spontaneous nature of the phenomenon of adsorption. When the temperature decreased from 318 to 288 K, the magnitude of $\Delta G°$ shifted to a high negative value from 2.90 to 4.76 kJ mol^{-1} using $MgFe_2O_4$ NPs as adsorbent, indicating that the process was more spontaneous at lower temperature. A similar trend was observed in the case of $CoFe_2O_4$ NPs and activated charcoal. The values of $\Delta H°$ were −23.49, −18.53 and −12.83 kJ mol^{-1} for $MgFe_2O_4$, $CoFe_2O_4$ NPs and activated charcoal, respectively. The negative entropy change ($\Delta S°$) value −64.76, −50.31 and −35.49 kJ mol^{-1} K^{-1} for $MgFe_2O_4$, $CoFe_2O_4$ NPs and activated charcoal, respectively was due to the lowering of the degrees of freedom of the adsorbed species.

3.2e *Adsorption isotherm study*: The equilibrium adsorption data obtained from the adsorption experiments was fitted in the Langmuir, Freundlich and D–R adsorption isotherms at two different temperatures i.e., 15 and 30°C. C_e/q_e *vs.* C_e was plotted to study Langmuir isotherm model and showed a straight line for ferrite NPs and activated charcoal conforming the fitting of Langmuir model at both temperatures (figure 9a and b). The value of q_{max} displayed a two-fold increase for $MgFe_2O_4$ and $CoFe_2O_4$ NPs as compared to activated charcoal indicating their better adsorption potential (table 4a and b). The value of q_{max} increased in the case of activated charcoal from 100 to 142.86 mg g^{-1} on lowering the temperature suggesting that its removal efficiency was enhanced at lower temperature. However in the case of $MgFe_2O_4$ and $CoFe_2O_4$, the q_{max} values remained same although percentage removal data indicated enhanced adsorption at 15°C. This can be corroborated with the fact that percent removal data

Table 3. Thermodynamic parameters (a) ln K and $\Delta G°$ and (b) $\Delta S°$ and $\Delta H°$ for Pb(II) ion adsorption.

	Adsorbent					
	$MgFe_2O_4$		$CoFe_2O_4$		Activated charcoal	
T (K)	ln K (mg l^{-1})	$\Delta G°$ (kJ mol^{-1})	ln K (mg l^{-1})	$\Delta G°$ (kJ mol^{-1})	ln K (mg l^{-1})	$\Delta G°$ (kJ mol^{-1})
(a)						
288	1.99	−4.77	1.65	−3.97	1.11	−2.66
298	1.73	−4.29	1.48	−3.67	0.89	−2.21
308	1.32	−3.39	1.15	−2.90	0.70	−1.81
318	1.09	−2.90	0.94	−2.40	0.61	−1.62

	Adsorbent		
	$MgFe_2O_4$	$CoFe_2O_4$	Activated charcoal
(b)			
$\Delta H°$ (kJ mol^{-1})	−23.49	−18.53	−12.83
$\Delta S°$ (kJ mol^{-1} K^{-1})	−64.76	−50.31	−35.49

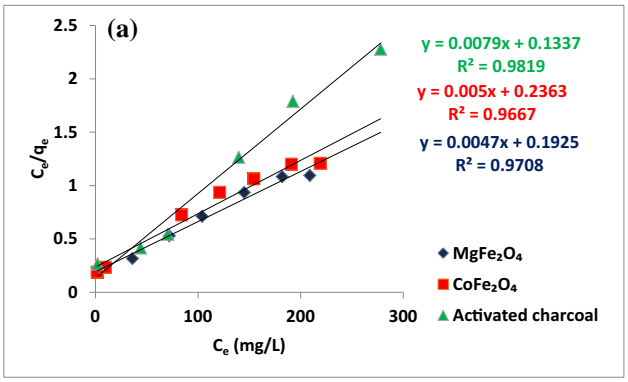

Figure 9. Langmuir isotherms of $MgFe_2O_4$, $CoFe_2O_4$ and activated charcoal at (**a**) 15°C and (**b**) 30°C.

gives actual behaviour of the adsorption under experimental conditions whereas q_{max} values were calculated theoretically from Langmuir plot. High value of correlation coefficient R^2 for $MgFe_2O_4$/$CoFe_2O_4$ NPs and activated charcoal indicated that Langmuir model of unimolecular layer adsorption fitted well in the experimental data.

Furthermore, a plot of log q_e *vs.* log C_e also displayed linear fitting for the three adsorbents used at 30 and 15°C which indicated that the data conform to the Freundlich model (figure 10a and b). However, from these plots it was evident that value of correlation coefficient (R^2) was higher for $MgFe_2O_4$ and $CoFe_2O_4$ NPs as compared to activated charcoal. In the case of activated charcoal, the value of correlation coefficient was 0.82 and 0.77 at 15 and 30°C respectively indicating that activated charcoal displayed better fit in Langmuir isotherm model than Freundlich isotherm model. The values of K_f and $1/n$ have been computed from these plots and recorded in table 4.

Furthermore, the adsorption data was applied to D–R isotherm model in order to understand the mechanism of adsorption. The value of D–R constants, β and Q_m were computed from these plots and recorded in table 4a and b. From the constant k, E was calculated, which was then used to estimate the mechanism of adsorption. From the D–R plots, the calculated value of E was 1.69, 1.41 and 1.21 at 30°C and 5.00, 5.42 and 1.30 at 15°C for $CoFe_2O_4$, $MgFe_2O_4$ and activated charcoal respectively which indicated that the adsorption was purely physical in nature [35]. But the lower values of correlation coefficient (0.752 to 0.892) suggested that the D–R model was not perfectly followed.

Pb(II) ions are adsorbed on the surface of ferrite NPs by weak van der Waals forces existing between O^{2-} ions forming lattice structures of ferrite NPs and Pb(II) ions. The presence of physisorption was confirmed by good fitting of Langmuir isotherm. The thermodynamic studies also revealed that the adsorption process was exothermic with negative ΔH values. A decrease in adsorption was observed with increase in temperature which confirmed physisorption.

3.2f *Conductance measurement*: Adsorption of Pb(II) ions on $MgFe_2O_4$ NPs was confirmed by recording the conductance of solution before and after adsorption. The conductance of 100 mg l^{-1} Pb(II) solution before adsorption was 0.139×10^{-3} ohm^{-1} and after adsorption, the eluent displayed a conductance value of 0.194×10^{-3} ohm^{-1}. This increase

Table 4. Langmuir, Freundlich and D–R parameters of $MgFe_2O_4$ and $CoFe_2O_4$ at (a) 15°C and (b) 30°C.

Composition	Langmuir constants			Freundlich constants			D–R constants			
	q_{max} (mg g^{-1})	$b \times 10^{-2}$(mg l^{-1})	R^2	K_f	N	R^2	β	Q_m (mg g^{-1})	E	R^2
(a)										
$MgFe_2O_4$	200.0	3.40	0.98	49.54	4.25	0.94	0.017	119.70	5.42	0.77
$CoFe_2O_4$	200.0	2.31	0.97	9.14	1.74	0.94	0.023	109.83	5.00	0.75
Activated charcoal	142.86	4.60	0.98	9.53	1.96	0.82	0.294	97.80	1.30	0.86
(b)										
$MgFe_2O_4$	200.0	2.60	0.98	52.60	4.50	0.93	2.191	131.76	1.69	0.89
$CoFe_2O_4$	200.0	1.77	0.95	7.24	1.68	0.94	0.249	103.13	1.41	0.81
Activated charcoal	100.0	8.50	0.98	8.63	2.09	0.76	0.339	82.85	1.21	0.87

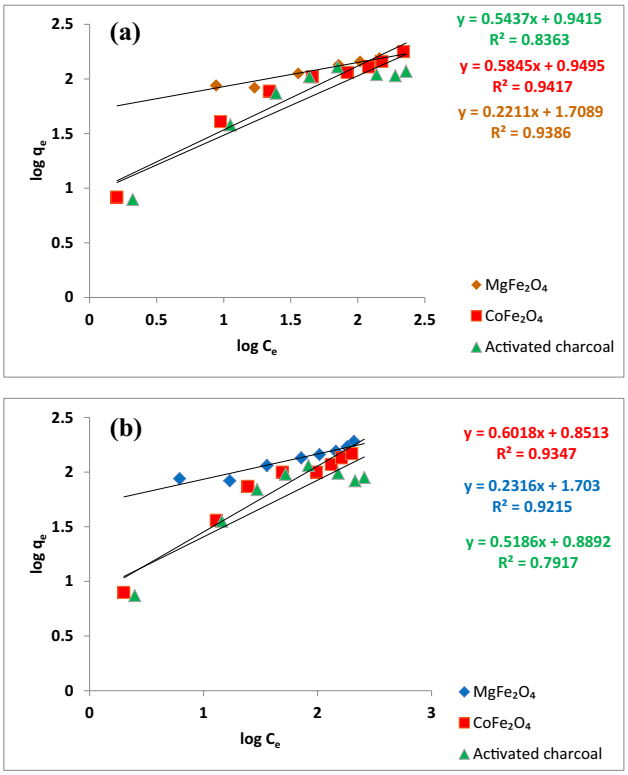

Figure 10. Freundlich isotherms of $MgFe_2O_4$, $CoFe_2O_4$ and activated charcoal at (**a**) 15°C and (**b**) 30°C.

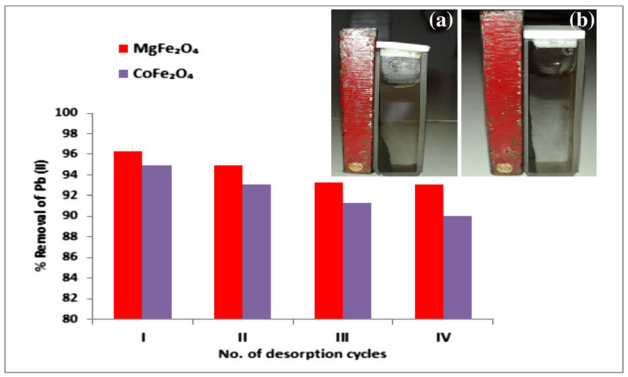

Figure 11. Plot of Pb(II) removal *vs.* desorption cycle and magnetic separation (inset).

in conductance indicated the absence of some of the Pb(II) ions in the eluent solution which confirmed the adsorption of Pb(II) ions on $MgFe_2O_4$ NPs. As the concentration of solution decreased due to adsorption, conductance increased because of rapid movement of the remaining ions. $CoFe_2O_4$ NPs and activated charcoal also displayed a similar decrease in solution conductance after adsorption but the decrease was lesser than $MgFe_2O_4$ NPs.

3.3 *Correlation between magnetic and structural properties and adsorption potential*

Adsorption data for MFe_2O_4 (M = Mg/Co) indicated a higher adsorption capacity of $MgFe_2O_4$ NPs as compared to $CoFe_2O_4$ NPs under similar conditions of temperature and pH. Conductance measurements also confirmed superiority of $MgFe_2O_4$ NPs although TEM micrographs revealed that the particle diameter of both the nanoadsorbents was similar. These observed results can be correlated to the magnetic behaviour of the synthesized ferrite NPs. A higher saturation magnetization of $CoFe_2O_4$ favoured greater agglomeration of NPs and formation of clusters, thus reducing the surface available for adsorption whereas, lower density of $MgFe_2O_4$ NPs is another reason for its better performance. Lower density resulted in a greater number of ferrite units per unit weight as compared to $CoFe_2O_4$ NPs, thus providing more active surface sites for adsorption. $MgFe_2O_4$ NPs not only have superior adsorptive properties, but are also more suitable for practical applications as Mg- and Ca-based spinel ferrites are reported to be biocompatible and safe [36].

3.4 *Desorption studies*

The separation of the prepared NPs from the solution using an ordinary magnet was an important aspect of this study (figure 11, inset). Desorption was carried out using solutions of 0.1 N HCl and 0.1 N HNO_3 and HCl was observed to be a better stripping solution. It was found that the removal efficiency of regenerated NPs was retained after successive

adsorption–desorption cycles (figure 11). $MgFe_2O_4$ and $CoFe_2O_4$ NPs showed percentage removal of 93 and 91% for Pb(II) ions even after four cycles which confirmed the reusability of NPs after facile magnetic separation.

4. Conclusions

MFe_2O_4(M = Mg, Co) NPs were synthesized by a facile combustion route which serves as a promising approach for bulk synthesis of NPs. The trend for the percentage removal of the Pb(II) ions was $MgFe_2O_4$ NPs > $CoFe_2O_4$ NPs > activated charcoal. The present study confirmed that the structure of spinel ferrite NPs can have significant impact on their adsorptive properties. The results were correlated to the density and magnetic parameters of ferrite NPs. Striking features of the nano-ferrites were the two-fold increase in q_{max} values and easy magnetic separation as compared to activated charcoal, thus confirming their better adsorption potential. $MgFe_2O_4$ NPs also have an edge over $CoFe_2O_4$ NPs due to their higher adsorption capacity uptake and the presence of non-toxic divalent Mg^{2+} ions.

References

[1] Harrison R M and Laxen D P H 1980 *Chem. Br.* **16** 316
[2] Perk M V 2006 *Soil and water contamination* (London, UK: Taylor and Francis Group plc) p 125
[3] Zhu S, Hou H and Xue Y 2008 *Appl. Clay Sci.* **40** 171
[4] Goel J, Kadirvelu K and Garg V K 2005 *J. Hazard Mater. B* **125** 211
[5] Pehlivan E and Atlun T 2007 *J. Hazard. Mater.* **140** 299
[6] Argun M E, Dursun S, Ozdemir C and Karatas M 2007 *J. Hazard. Mater.* **141** 77
[7] Chen Q, Luo Z, Hills C, Xue G and Tyrer M 2009 *Water. Res.* **43** 2605
[8] Bhatnagar A and Minocha A K 2006. *Chem. Technol.* **13** 203
[9] Seo S H, Sung B W, Kim G J, Chu K H, Um C Y, Yun S L *et al* 2010 *Water Sci. Technol.* **62** 2115
[10] Khaleel A, Kapoor P N and Klabunde K J 1999 *Nanostruct. Mater.* **11** 459
[11] Kaur M, Rana S and Tarsikka P S 2012 *Ceram. Int.* **38** 4319
[12] Kaur M, Kaur N and Vibha 2016 in *Ferrites and ferrates: chemistry and applications in sustainable energy and environmental remediation* V Sharma (ed) (American Chem. Soc., Washington, DC) p 113
[13] Hou X, Feng J, Liu X, Ren Y, Fan Z, Wei T *et al* 2011 *J. Colloid. Interface Sci.* **362** 477
[14] Kuai S, Zhang Z and Nan Z 2013 *J. Hazard. Mater.* **250** 229
[15] Hu J, Lo I M C and Chen G 2007 *Sep. Purif. Technol.* **56** 249
[16] Lagashetty A, Vijyanand H, Basavaraja S, Mallikarjuna N N and Venkataraman A 2010 *Bull. Mater. Sci.* **33** 4
[17] Ren Y, Li N, Feng J, Luan T, Wen Q, Li Z *et al* 2012 *J. Colloid. Interface Sci.* **367** 415
[18] Bakshayesh S and Dehghani H 2014 *J. Iran. Chem. Soc.* **11** 769
[19] Reddy D H K and Lee S 2013 *Ind. Eng. Chem. Res.* **52** 15789
[20] Culita D C, Simonescu C M, Patescu R E, Dragne M, Stanica N and Oprea O 2016 *J. Solid State Chem.* **238** 311
[21] Culita D C, Simonescu C M, Dragne M, Stanica N, Munteanu C, Preda S *et al* 2015 *Ceram. Int.* **41** 13553
[22] Fang B, Yan Y, Yang Y, Wang F, Chu Z, Sun X *et al* 2016 *Water Sci. Technol.* **73** 1112
[23] Kang D, Yu X, Ge M F and Song W 2015 *Microporous Mesoporous Mater.* **207** 170
[24] Kaur M, Kaur N, Jeet K and Kaur P 2015 *Ceram. Int.* **411** 3739
[25] Kaur M, Singh M, Mukhopadhyay S S, Singh D and Gupta M 2015 *J. Alloys Compd.* **653** 202
[26] Christian G D 2004 *Analytical chemistry* (New Jersey, USA: John Wiley and Sons Inc.)
[27] Lagashetty A and Venkataraman A 2004 *Bull. Mater. Sci.* **27** 491
[28] Nabiyouni G, Fesharaki M J, Mozafari M and Amighian J 2010 *Chin. Phys. Lett.* **27** 126401
[29] Klug H P and Alexander I 1962 *X-ray diffraction procedure* (New York: Wiley)
[30] ASTM Card No. 17-484
[31] Maensiri S, Sangmanee M and Wiengmoon A 2009 *Nanoscale Res. Lett.* **4** 221
[32] Arulmurugan R, Jeyadevan B, Vaidyanathan G and Sendhilnathan S 2005 *J. Magn. Magn. Mater.* **288** 470
[33] Kaur M, Jain P and Singh M 2015 *Mater. Chem. Phys.* **162** 332
[34] Pang Y, Zeng G, Tang L, Zhang Y, Liu Y, Lei X *et al* 2011 *Desalination* **281** 278
[35] Tang L, Yang G D, Zeng G M, Cai Y, Li S S, Zhou Y Y *et al* 2014 *Chem. Eng. J.* **254** 302
[36] Kaur M and Kaur M 2018 *Ceram. Int.* **44** 4158